Available online at www.sciencedirect.com
ScienceDirect
Trans. Nonferrous Met. Soc. China 25(2015) 2446−2457
Transactions of Nonferrous Metals Society of China
www.tnmsc.cn

Electrochemical migration behavior and mechanism of PCB-ImAg and PCB-HASL under adsorbed thin liquid films

Kang-kang DING, Xiao-gang LI, Kui XIAO, Chao-fang DONG, Kai ZHANG, Rui-tao ZHAO

Corrosion and Protection Center, University of Science and Technology Beijing, Beijing 100083, China

Received 2 September 2014; accepted 20 November 2014

Abstract: The electrochemical migration (ECM) behavior and mechanism of immersion silver processing circuit board (PCB-ImAg) and hot air solder leveling circuit board (PCB-HASL) under the 0.1 mol/L Na_2SO_4 absorbed thin liquid films with different thicknesses were investigated using stereo microscopy and scanning electron microscopy (SEM). Meanwhile, the corrosion tendency and kinetics rule of metal plates after bias application were analyzed with the aid of electrochemical impedance spectroscopy (EIS) and scanning Kelvin probe (SKP). Results showed that under different humidity conditions, the amount of migrating corrosion products of silver for PCB-ImAg was limited, while on PCB-HASL both copper dendrites and precipitates such as sulfate and metal oxides of copper/tin were found under a high humidity condition (exceeding 85%). SKP results indicated that the cathode plate of two kinds of PCB materials had a higher corrosion tendency after bias application. An ECM model involving multi-metal reactions was proposed and the differences of ECM behaviors for two kinds of PCB materials were compared.

Key words: immersion silver processing circuit board (PCB-ImAg); hot air solder leveling circuit board (PCB-HASL); electrochemical migration; electrical bias; absorbed thin liquid film

1 Introduction

With the innovation of electronic technology, integration and miniaturization become the future developing direction for printed circuit board (PCB). Meanwhile, the corrosion problems of PCB also stand out more clearly, and even trace amounts of corrosion products will have a serious impact on the reliability of PCB [1]. Under the actual environment for use, due to the diurnal temperature variations or/and the temperature field fluctuations for PCB itself, condensation phenomenon is prone to occur. As a result, a thin layer of absorbed thin liquid film (<10 μm) whose thickness changes dynamically with the working conditions, will be formed on the surface of PCB, causing electrochemical corrosion under dynamic thin liquid films. Especially, when applied with an electrical bias, ions will migrate directly between conductors, which will result in electrochemical migration (ECM) corrosion and significantly increase the risk of a short-circuit failure for PCB [2]. ECM includes two forms: conductive anode filaments (CAFs) and dendrites growth [3]. A CAF is a filamentous conductive path formed as anode metals become ionized and begin to migrate. This process is driven by an applied electric field from the anode to the cathode [4]. READY and TURBINI [5] studied systematically the effects of flux chemistry, applied voltage (V), spacing (L) and temperature on the forming rate of CAFs and found that the mean time to a short-circuit failure was a function of L^4/V^2. Dendrite growth occurs as a result of metal ions going into solution at the anode and plating out at the cathode, growing in needle- or tree-like formations. Generally, a incubation period is needed for dendrites growth [6,7].

Since copper and its alloys have many excellent properties, such as good electrical and thermal conductivity, low cost and high reliability of solder joints [8], they are widely used as the substrate materials of PCB. However, Cu is prone to oxidation or corrosion [9,10]. In order to improve the corrosion resistance of PCB materials, surface treatments are usually applied in their actual use, among which immersion silver (ImAg) and hot air solder leveling (HASL) technologies get wide range of applications due to their superior corrosion resistance and good weldability [11]. As an emerging technology for ImAg, rusting of the ImAg layer and ECM phenomenon [12] is the most commonly

Foundation item: Project (51271032) supported by the National Natural Science Foundation of China
Corresponding author: Kui XIAO; Tel: +86-10-62333975-522; E-mail: xiaokui@sina.com
DOI: 10.1016/S1003-6326(15)63861-4

encountered problem in the practical application environment for immersion silver processing circuit board (PCB-ImAg). YANG and CHRISTOU [13] proposed an ECM failure model about the Ag plating layer based on the experimental data and a systematic summary of previous work, and pointed out that ECM process of Ag required a long time of ions accumulation stage, which is closely related to temperature, humidity, electrical bias and material properties. Another surface technology, i.e., HASL technology, occupies an important position in the PCB industry due to its low cost. Currently, growth of Sn whiskers [14,15] and fretting corrosion [16] are the research hotspots about the corrosion of hot air solder leveling circuit board (PCB-HASL) materials. However, the ECM problems cannot be ignored for PCB-HASL, as LEE et al [17] once found that the CAFs near 63Sn−37Pb solder on PCB could lead to a serious short-circuit failure. A series of studies have compared the ECM susceptibility of different metallization systems, and generally they can be ranked as Ag>Pb>Cu>Sn [18,19].

Generally, surface plating treatments can provide good protection on the metal substrate from corrosion. However, as a result of the usage of plating metals, a multi-metal system for PCB is formed, which may increase the risk of ECM corrosion failure due to the different ECM characteristics of metals. Presently, related researches mainly focus on the prediction of time-to-failure or probability of failure, while the roles of different metals (including the substrate and the plating metals) in the ECM process need to be further distinguished. In this work, stereo microscopy, scanning electron microscopy (SEM), X-ray energy dispersive spectrometer (EDS), scanning Kelvin probe (SKP) and electrochemical impedance spectroscopy (EIS) techniques were used to study the ECM behavior and mechanism of PCB-ImAg and PCB-HASL under 0.1 mol/L Na_2SO_4 thin liquid films (to simulate the sulfur-containing atmosphere environment) with different thicknesses and an ECM model involving multi-metal reactions was proposed. This work can provide the data base and guidance for the selection and life assessment for PCB usage under the actual service environment.

2 Experimental

2.1 Materials preparation

PCB-ImAg and PCB-HASL were chosen as the experimental materials, whose basic processing parameters are shown in Table 1. The effective sizes of single metal plates are 3 mm×30 mm, and the spacing between two neighbor plates is 0.2 mm. The board materials are FR-4 epoxy glass cloth. Before experiment, the samples were dealt as follows: ultrasonic cleaning in acetone for 10 min, ultrasonic washing in deionized water for another 10 min, scrubbing with ethanol and then drying naturally.

2.2 Damp heat test coupled with voltage

0.1 mol/L Na_2SO_4 solution was chosen as the electrolyte, and with the aids of a medical spray gun a certain amount (approximately 0.1 mL) of Na_2SO_4 droplets were uniformly sprayed on the sample surface to simulate the condensation phenomenon under a sulfur-containing atmospheric environment. Then, the samples were placed in the damp heat cabinet (ESPEC SET-Z−022R), where the temperature was controlled at 60 °C, while the relative humidity values were set as 75%, 85% and 95% (corresponding to different thicknesses of absorbed thin liquid films), respectively. After a layer of stable thin liquid film was formed on the surface (after 1 h), an electrical bias of 12 V was applied between two neighbor plates for 24 h. Then, the electrical bias was eliminated and the samples were taken out for further test. The left of the experimental materials is cathode plate, and the right is anode plate. All the following experiments were carried out in a stable laboratory environment of 25 °C and 60% relative humidity (RH).

2.3 Experimental methods

Stereo microscope (Keyence VHX−2000) and environment scanning electron microscope (ESEM, FEI Quanta 250) were used to observe the ECM corrosion morphology. Combined with EDS analyzer, the distribution of elements between two neighbor plates was detected. Volta potentials of the sample surfaces were measured using M370 scanning Kelvin probe with a work distance of (100±2) μm. The scanning area is in sizes of 4 mm × 3 mm, sweeping from the cathode to the anode plate with step size of 100 μm along *x*-axis direction and 200 μm along *y*-axis direction.

The PARSTAT 2273 electrochemical workstation was taken as the EIS measuring instrument and a micro-electrode system shown in Fig. 1 was set: a region of 0.0025 cm^2 on the edge of the cathode plate as the working electrode, a platinum wire as the auxiliary electrode and a saturated calomel electrode (SCE) as the

Table 1 Basic processing parameters of PCB

Board No.	Board material	Board thickness/mm	Thickness of copper foil/μm	Surface treatment	Thickness of protective layer/μm
1	FR-4	2	25−30	ImAg	0.02
2	FR-4	2	25−30	HASL	10

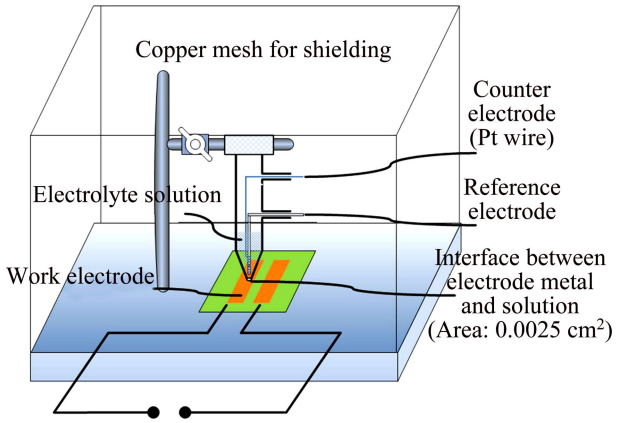

Fig. 1 Schematic diagram of micro-electrode system and EIS measurement [15]

reference electrode. EIS measurement was conducted under the open-circuit potential in 0.1 mol/L Na_2SO_4 electrolyte solution, with a scanning frequency from 100 kHz to 10 mHz and a disturbance potential of 10 mV. After finishing the test, ZSimpWin V3.20 was applied for EIS data fitting. Each test repeated three times.

3 Results and discussion

3.1 Corrosion morphology observation

The corrosion morphologies of PCB after bias application for 24 h under experimental conditions are shown in Fig. 2. As can be seen from Fig. 2(a_1), the ECM corrosion for PCB-ImAg was relatively slight under 75% RH. The ImAg layer on the cathode plate only had a slight discoloration, in light brown, which might be caused by the surface oxidation reactions (Ag_2O as well as little Ag_2S/Ag_2SO_4 perhaps) [20,21], while the anode plate was smooth without any significant change. With the increase of the relative humidity, the color of the cathode plate gradually deepened, and a severe enrichment phenomenon of salt occurred on the sample surface (white regions). Meanwhile, the anode plate surface also became rough, showing a brown color in localized regions where oxidation/corrosion occurred. Furthermore, the corrosion of the anode plate edge was much serious, where a large amount of green corrosion products, presumably "patina", were accumulated with a limited migration distance.

Different from PCB-ImAg, severe corrosion happened on the PCB-HASL cathode plate under 75% RH (Fig. 2(a_2)). When the relative humidity exceeded 85%, a large amount of green corrosion products began to accumulate in the central region between two plates, forming a boundary. On the right side (near the anode side) of this boundary, there were a lot of red-brown substances which were presumably Cu dendrites and might cause a short-circuit failure. Meanwhile, the corrosion regions of the cathode plate expanded significantly, and the enrichment condition of salt was also exacerbated.

3.2 Corrosion products analysis

To explore the ECM behavior and mechanism of PCB, the element distribution mapping detection between two plates after bias application was performed, as shown in Fig. 3. As could be seen from Fig. 3(b), obvious migration occurred for Cu element, which developed from the anode to the cathode plate and nearly half of the FR-4 board was covered. Meanwhile, trace amounts of Ag element were detected in the coverage region of Cu element (Fig. 3(c)), but no obvious Ag dendrites were found under all the experimental conditions, which might be related to the fact that Ag had

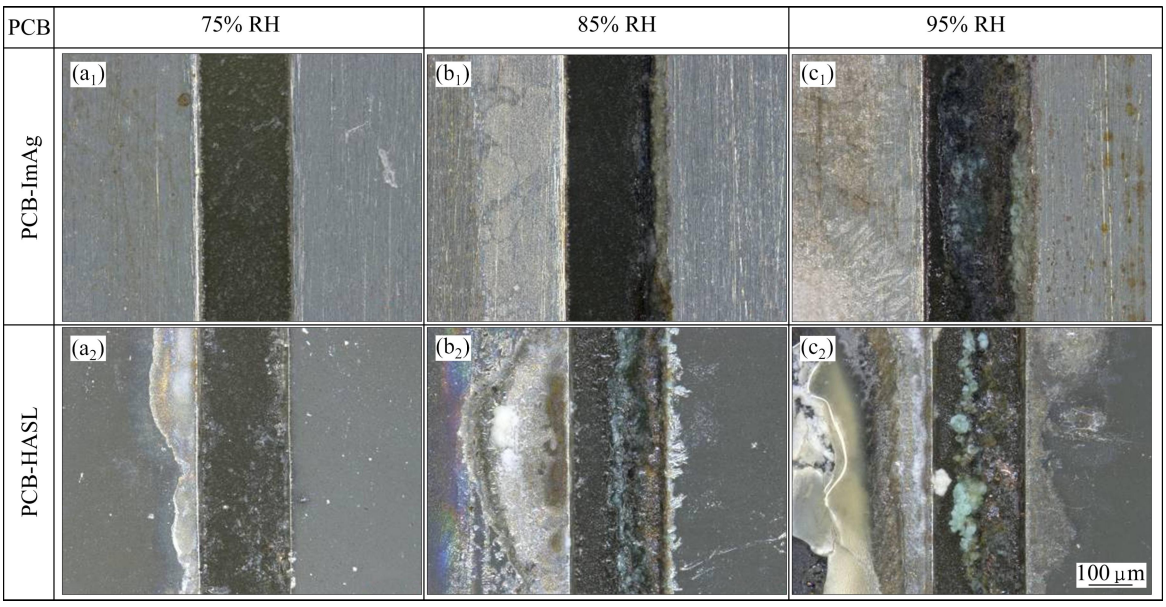

Fig. 2 Stereo micrographs of PCB after bias application under different experimental conditions

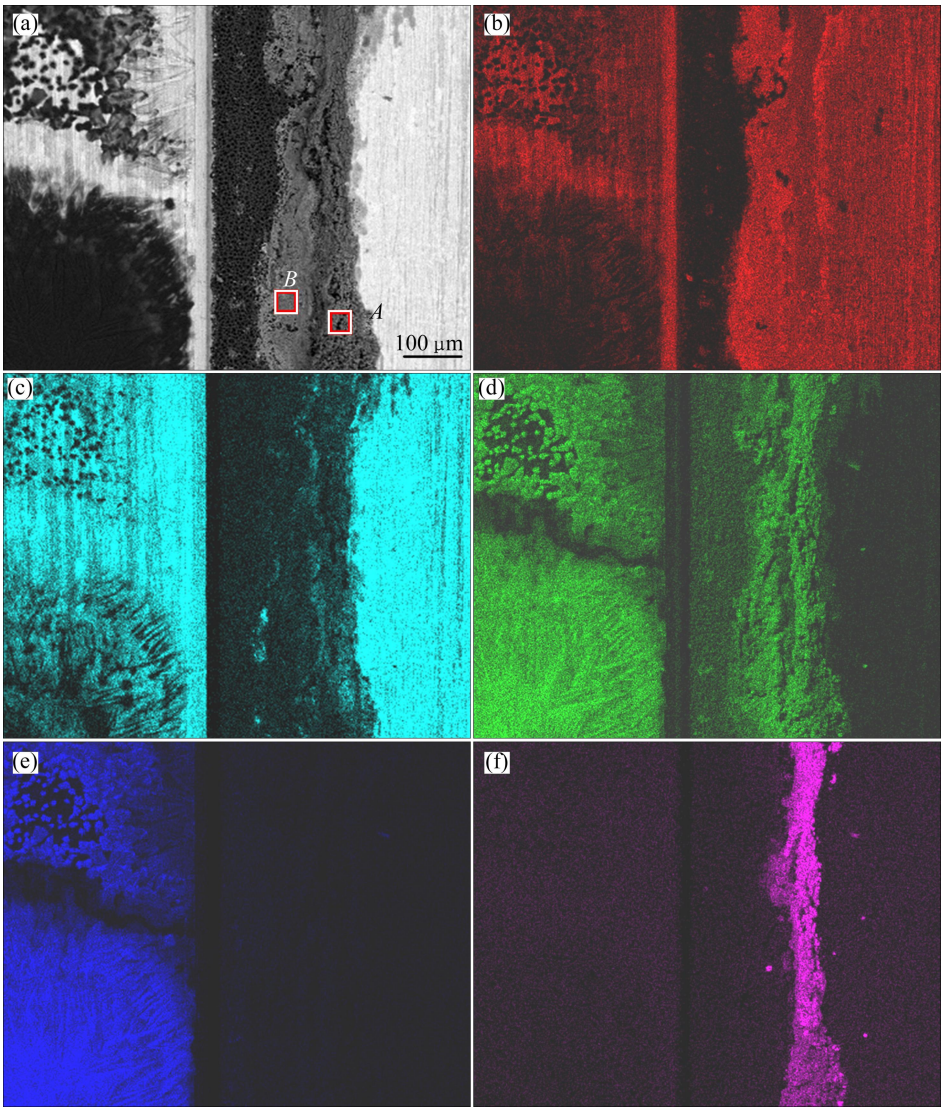

Fig. 3 Element distribution mapping results for PCB-ImAg after bias application in environment of 60 °C and 95% RH: (a) SEM image; (b) Cu; (c) Ag; (d) O; (e) Na; (f) S

a lower corrosion susceptibility or ECM tendency under SO_2/SO_4^{2-} environment [1]. From Fig. 3(a), it could be found that the migration substances were divided into two parts: for the back part which was close to the anode plate, accumulation of corrosion products was serious, and O and S elements were enriched as shown in Figs. 3(d) and (f), indicating that the corrosion products were possibly sulfates of Cu; in contrast, only the content of O element was high for the front part (Area *B*), where the corrosion products should be oxides or hydroxides of Cu, which was consistent to the EDS analysis results in Table 2. Furthermore, Fig. 3(e) showed that Na element was gathered on the surface of the cathode plate, where the content of O element also increased significantly (Fig. 3(d)). Therefore, it can be speculated that the reaction occurring on the cathode plate is primarily the oxygen reduction reaction and the composition of the salt should be NaOH.

The element distribution mapping results for PCB-HASL are shown in Fig. 4. From Fig. 4(b), Cu dendrites could be seen clearly on the FR-4 board near the anode plate. Judging from the growing direction and position, Cu ions from the anodic dissolution only migrated into the central position between two plates and began to deposit as dendrites of reverse growth.

Figure 4(c) showed that Sn element was gathered on the FR-4 board adjacent to the cathode plate. According to the EDS results of Area *C* shown in Table 2, the substance containing Sn element should be mainly composed of oxides or hydroxides of Sn. Simultaneously, a certain amount of metal Sn might also exist, thus it had certain conductivity, which could explain the reason why Cu dendrites growth started from the central position between two plates. From Fig. 4(b), it could be further

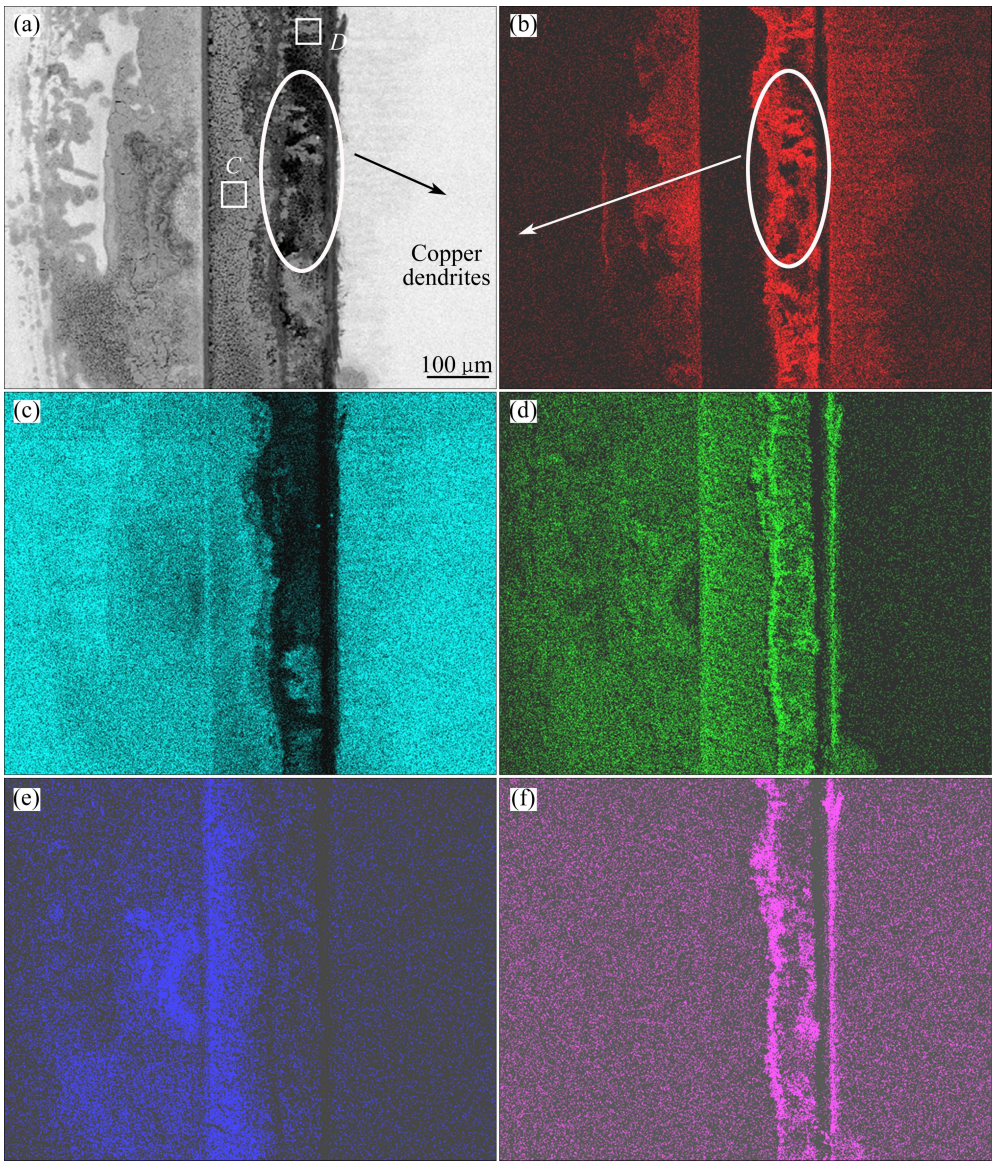

Fig. 4 Element distribution mapping results for PCB-HASL after bias application in environment of 60 °C and 95% RH: (a) SEM image; (b) Cu; (c) Sn; (d) O; (e) Na; (f) S

Table 2 EDS results of migrating corrosion products for PCB-ImAg and PCB-HASL

Area	Mole fraction/%						
	C	O	Al	S	Ag	Sn	Cu
A in Fig. 3(a)	13.32	47.66	−	−	−	−	39.02
B in Fig. 3(a)	4.49	49.76	−	9.09	5.08	−	31.58
C in Fig. 4(a)	8.99	57.47	1.48	0.11	−	19.90	12.04
D in Fig. 4(a)	24.96	27.53	4.82	1.33	−	1.3	40.06

found that the content of Cu element in the edge regions of the anode and cathode plates increased to some extent, indicating that the Sn plating layer was thinned. Thus, it could be concluded that part of the Sn corrosion products at the vicinity of the cathode plate might be from the Sn dissolving and ions migrating process on the anode plate, while the other part came from the Sn dissolving and re-precipitating process on the cathode plate under the effect of high concentration OH^-. Furthermore, the directional migration and enrichment phenomenon of Na and S elements occurred, which was similar to the condition of PCB-ImAg. The difference was that S element also gathered at the central position between two plates, along with a significant increase of Cu and O contents, reflecting that a large amount of Cu sulphate precipitates were generated at this position.

3.3 SKP analysis

In order to observe the change of surface potential states for the cathode and anode plates and explore the corrosion behavior and rules under non-working state for voltage parts, the surface Kelvin potentials (φ_{kp}) of PCB after bias application were measured. The principle of the Kelvin probe techniques is to determine the contact

potential difference by measuring the electronic work function of metal surface in air. This potential has a linear relationship with the surface potential (φ_{corr}) in air (Eq. (1)) [22−24]:

$$\varphi_{corr}=\left(\frac{W_{ref}}{F}-\frac{\varphi_{ref}}{2}\right)+E_{kp} \quad (1)$$

where W_{ref} is the electrode work function, and $\varphi_{ref}/2$ is the half-cell potential of the reference electrode (vibrating probe). These two parameters are constant under a specific system. Thus, the change of φ_{kp} reflects the change of the surface potential.

Gauss fitting was carried out on the surface Kelvin potential distribution of the anode and cathode plates, respectively. The fitting formula is shown as

$$y=y_0+\frac{A}{\sigma\sqrt{2\pi}}\exp\left(-\frac{(x-\mu)^2}{2\sigma^2}\right) \quad (2)$$

where μ is the expectation value of potential distribution φ_{kp}; σ is the standard deviation of the Gaussian distribution, which represents the dispersion degree of the potential distribution. The greater the σ value is, the more the dispersed potential distribution is.

As could be seen from Fig. 5, Fig. 6 and Table 3, the surface Kelvin potential distribution for PCB-ImAg under different humidity conditions exhibited a similar law that the potential of the anode plate was significantly higher than that of the cathode plate. This indicated that the surface states of the PCB-ImAg plates had been altered significantly, and the state changes would not disappear even after the elimination of the electrical bias. As the relative humidity increased, the potentials of the two plates showed a downward trend, but those of the cathode plates fell much more sharply. As a result, the potential difference between two plates continuously increased, and reached a maximum value of 0.5693 V under 95% RH. In combination with the corrosion morphologies shown in Fig. 2, it could be found that with the increase of humidity, a certain degree of rusting occurred in localized regions of the ImAg layers. However, the overall corrosion condition was relatively slight, thus the PCB-ImAg surface was in a state of activation. This would cause a decline of the surface electronic work function, as well as the surface Kelvin potentials subsequently, which was more obvious for the cathode plate. Furthermore, the accumulation of salts or corrosion products in the edge region of the cathode plates contributed to the uneven potential distribution of the whole cathode plate surface. As humidity increased, the uneven potentials distribution situation was further exacerbated, with σ gradually increasing from 0.0601 to 0.1568.

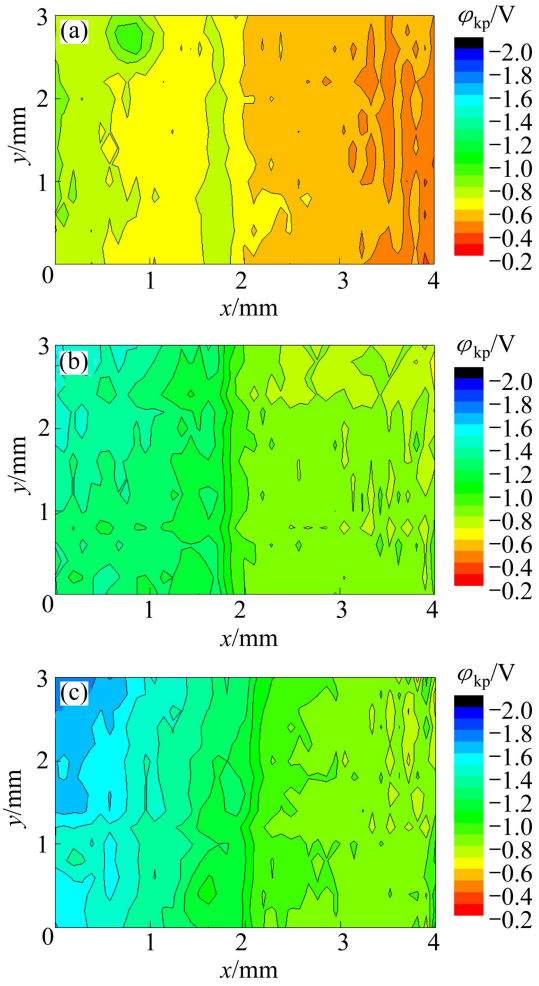

Fig. 5 Surface Kelvin potential distribution for PCB-ImAg after bias application under different experimental conditions: (a) 75% RH; (b) 85% RH; (c) 95% RH

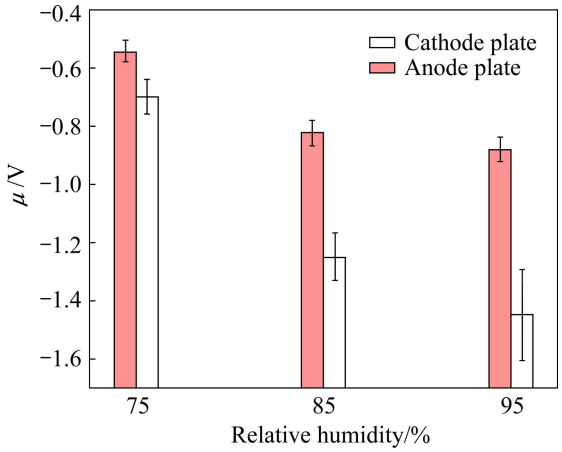

Fig. 6 Curves of potential expectations vs relative humidity for PCB-ImAg

As shown in Fig. 7, Fig. 8 and Table 4, the evolution rule of the surface Kelvin potential distribution for PCB-HASL was totally contrary to that of PCB-ImAg. As humidity increased, the potentials of

Table 3 Gauss fitting results of surface Kelvin potential distribution for PCB-ImAg

RH/%	Cathode plate		Anode plate	
	μ/V	σ	μ/V	σ
75	−0.6991	0.0601	−0.5419	0.0370
85	−1.2490	0.0821	−0.8240	0.0439
95	−1.4490	0.1568	−0.8797	0.0425

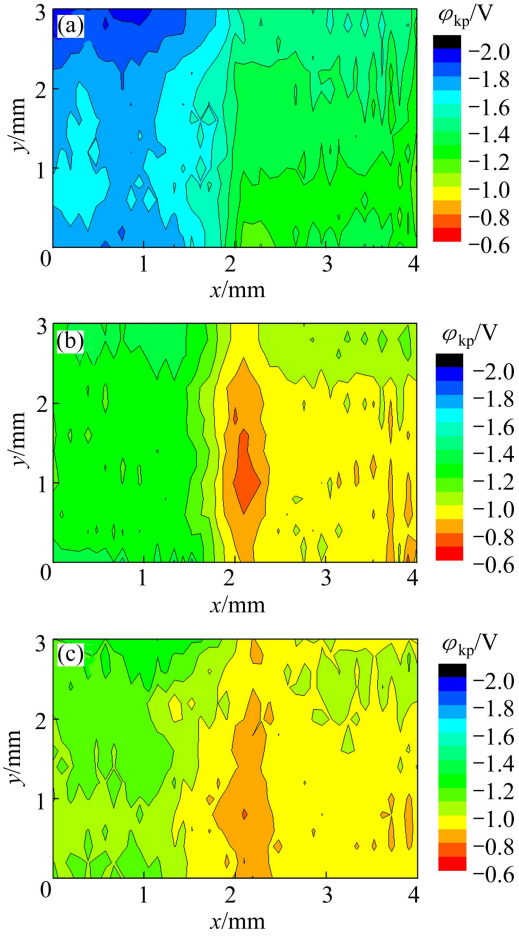

Fig. 7 Surface Kelvin potential distribution for PCB-HASL after bias application under different experimental conditions: (a) 75% RH; (b) 85% RH; (c) 95% RH

both plates showed an upward trend, while the potential difference between two plates decreased gradually, from 0.3701 to 0.1484 V. In the experimental medium (SO_2/SO_4^{2-}) environment, a layer of Sn oxide film (mainly composed of SnO, SnO_2, Sn $(OH)_2$ or Sn $(OH)_4$) [25] will be formed on the PCB-HASL surface, and under high humidity condition, the oxidation degree will be further exacerbated due to the increase of oxygen reduction reaction rates [26]. The existence of the oxide films hindered the electron emitting process and resulted in a continuous enhancement of the surface potentials. As mentioned above, the cathode plates for PCB-HASL were corroded more severely (Fig. 2), thus their

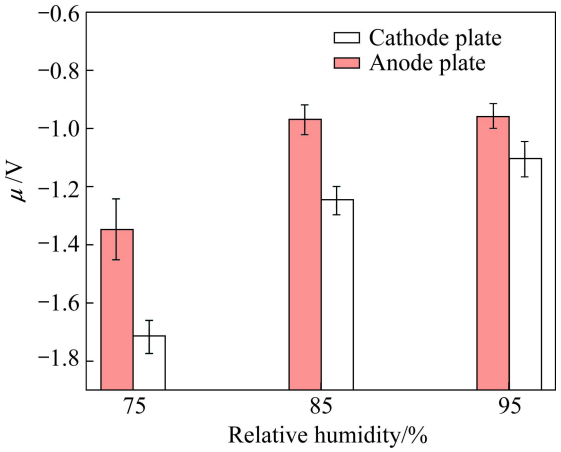

Fig. 8 Curves of φ_{kp} expectations vs relative humidity for PCB-HASL

Table 4 Gauss fitting results of surface Kelvin potential distribution for PCB-HASL

RH/%	Cathode plate		Anode plate	
	μ/V	σ	μ/V	σ
75	−1.7174	0.0578	−1.3473	0.1043
85	−1.2488	0.0490	−0.9716	0.0510
95	−1.1062	0.0613	−0.9578	0.0430

potentials increased more rapidly, which reduced the potential difference between two plates. Furthermore, due to the accumulation of a large amount of corrosion products in the central region between two plates, the surface Kelvin potential increased significantly, forming a distinct boundary which showed a warm color tone in the potential diagram (Figs. 7(b) and (c)).

Overall, the potential expectations of PCB-HASL were lower than those of PCB-ImAg, indicating that PCB-HASL had a higher corrosion tendency, but the potential difference between two PCB-HASL plates was much smaller. When a layer of electrolyte film is formed on the PCB surface, the large potential difference between two (micro) short-circuit plates will lead to the galvanic corrosion reaction. As a result, the voltage parts may still suffer severe corrosion damage under the non-working state. In this regard, the performance of PCB-HASL is superior to that of PCB-ImAg.

3.4 EIS measurement

To study the corrosion mechanism of the PCB plates and explore the protective effects of the corrosion product film or surface protection layer on the substrate, a micro-electrode system was set up for EIS measurements aiming at the cathode plate edge region where severe corrosion occurred after bias application, as shown in Fig. 9. As could be seen from Fig. 9(a), the Nyquist diagrams of PCB-ImAg samples under low

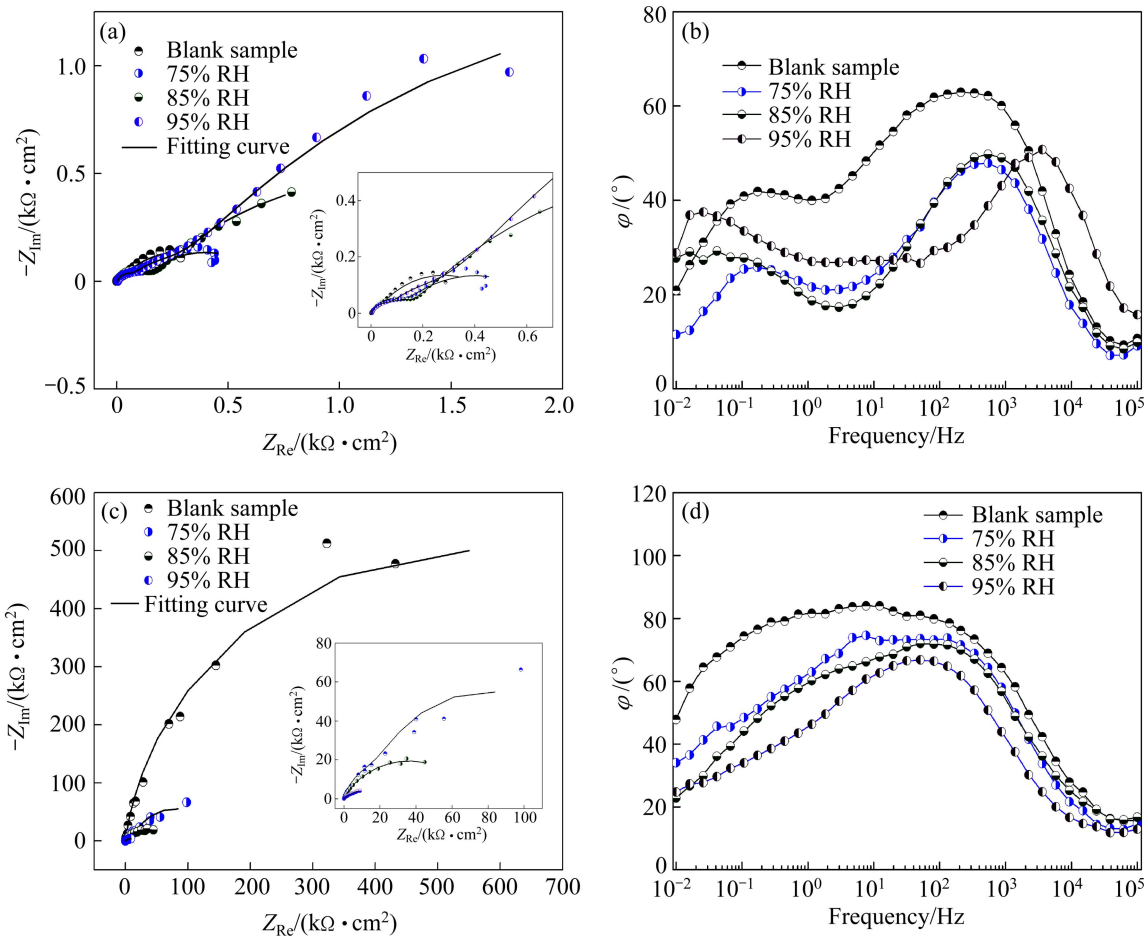

Fig. 9 EIS of PCB cathode plates after bias application: (a,b) Nyquist and Bode diagrams for PCB-ImAg, respectively; (c,d) Nyquist and Bode diagrams for PCB-HASL, respectively

humidity conditions (75%−85% RH, including the blank PCB-ImAg) consist of two capacitive arcs. Considering the existence of micropores and defects within the ImAg layer, the equivalent circuit shown in Fig. 10(a) was adopted to fit the EIS data. Wherein, R_s represents the solution resistance; CPE_f represents the film capacitance of the surface plating layer; R_f represents the resistance of solution or/and corrosion products within the micropores; CPE_{dl} and R_{ct} represent the electric double layer capacitance and the charge transfer resistance of the interface between the substrate and the electrolyte within the micropores, respectively. When the relative humidity reached 95%, due to the isolation effect of the thick layer of oxides or/and corrosion products film on the surface, the Nyquist diagram transformed into three capacitive arcs. In this case, the equivalent circuit shown in Fig. 10(b) was adopted. Wherein, R_o and CPE_o represent the resistance and film capacitor of the surface oxide film or/and corrosion product film, respectively. Generally, R_{ct} reflects the magnitude of the interface reaction resistance, which is often used to characterize the rate of the corrosion reaction. The larger the R_{ct} is, the smaller the corrosion rate is. The corresponding

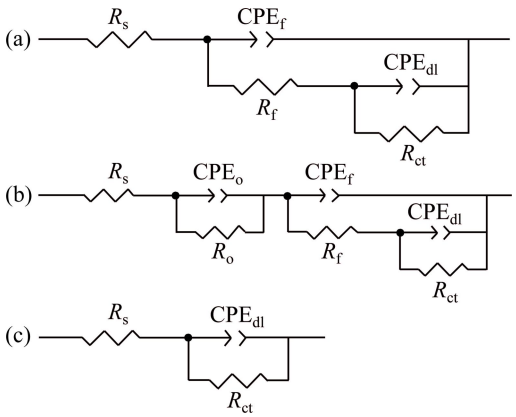

Fig. 10 Equivalent circuits for EIS fitting: (a) Blank PCB-ImAg and PCB-ImAg under 75%−85% RH as well as PCB-HASL under 75%−95% RH; (b) PCB-ImAg under 95% RH; (c) Blank PCB-HASL sample

fitting results of R_{ct} are shown in Fig. 11. As can be seen from Fig. 11, after bias application, R_{ct} of the cathode plate increased to some extent, indicating that the corrosion product played a protective role on the substrate through filling the micropores or defects in the ImAg layer.

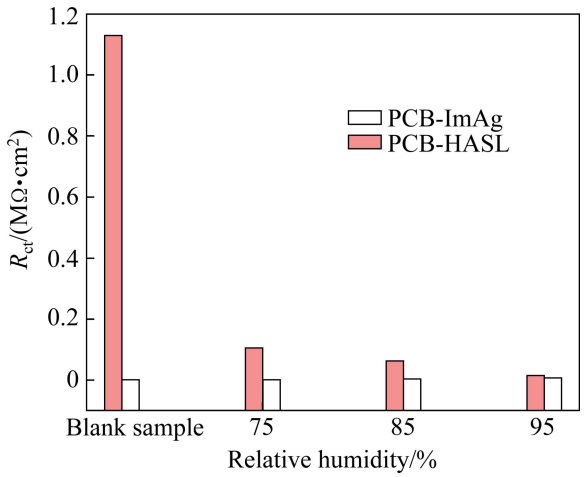

Fig. 11 Change of R_{ct} for PCB cathode plates after bias application relative humidity

Compared with PCB-ImAg, the thickness of the Sn plating layer for PCB-HASL is much larger (~10 μm). As a result, the electrolyte solution cannot directly contact with the substrate through the Sn plating layer. Therefore, EIS of the blank PCB-HASL mainly reflects the interface reaction information between the electrolyte solution and the Sn plating layer, and the equivalent circuit in Fig. 10(c) was adopted. After bias application, due to the accumulation of corrosion products on the surface of the cathode plate, EIS Nyquist diagrams transformed into two capacitive arcs. The high-frequency capacitive arc reflects the information of the layer of corrosion product film, while the low-frequency capacitive arc is closely related to the interfacial reaction process. In this case, the equivalent circuit shown in Fig. 10(a) was adopted again. Wherein, R_f and CPE_f represent the resistance and film capacitor of the surface oxide film or/and corrosion products film respectively. In combination with Fig. 11, it could be seen that R_{ct} reached the maximum value for the blank PCB-HASL since a thin layer of dense SnO_2 film formed in the air could effectively isolate the electrolyte solution from the substrate. After bias application, R_{ct} declined sharply, indicating that the generated corrosion product film had a loose structure and could not provide any protection on the substrate. When the relative humidity reached 95%, R_{ct} decreased to a value quite close to that of PCB-ImAg.

3.5 ECM mechanism

ECM under the absorbed thin liquid film is the main corrosion failure mechanism for PCB under the experimental conditions. For PCB-ImAg, the main anodic reactions may include Eqs. (3)−(5):

$$Ag \longrightarrow Ag^{+}+e \quad (3)$$

$$Cu \longrightarrow Cu^{+}+e \quad (4)$$

$$Cu^{+} \longrightarrow Cu^{2+}+e \quad (5)$$

The electrical bias applied in this test is relatively large (12 V), thus the metal ions from dissolving of copper-foil should be mainly Cu^{2+} (Cu^{+} will be further oxidized). Furthermore, a certain degree of decomposition of water will occur at such a voltage value, generating a small amount of H^{+} [27]. The reaction is shown as

$$2H_2O \longrightarrow O_2+4H^{+}+4e \quad (6)$$

The reactions happened on the cathode plate should mainly be reduction of O_2 or/and the decomposition of water. In addition, judging from the corrosion morphologies in Fig. 2, a weak anode reaction may also happen, forming a layer of brown Ag_2O film (little Ag_2S, Ag_2SO_4, etc.). Possible reactions on the cathode plate are shown as follows:

$$O_2+2H_2O \rightarrow 4OH^{-}-4e \quad (7)$$

$$2H_2O \rightarrow H_2+2OH^{-}-2e \quad (8)$$

$$Ag+OH^{-} \rightarrow AgOH+e \quad (9)$$

$$2AgOH \rightarrow Ag_2O+H_2O \quad (10)$$

As shown in Fig. 12, under the effect of the electrical bias, anions and cations migrate directionally and this situation is further exacerbated with an increase of humidity, resulting in the enrichment phenomenon of specific ions on two different plates, such as Na^{+} and SO_4^{2-}. On one hand, the thickness of the ImAg layer is very thin (only 0.02 μm) with a smaller charge number, and the quality of Ag^{+} (relative atom mass: 108) is larger than that of Cu^{2+} (relative atom mass: 64), which greatly limits the migration amount and migration velocity of Ag^{+}. On the other hand, the ECM process of Ag^{+} requires a long time of ions accumulation stage [13], while the galvanic dissolution reaction of the Cu substrate within the micropores or defects of the ImAg layer does not need any electrical bias. Therefore, the main migrating ions should be Cu^{2+} ions.

As time goes by, SO_4^{2-} ions gradually migrate and gather near the anode plate. Since the content of the aqueous medium on the surface of PCB-ImAg is quite limited, even in the condition of 95% RH, when a large number of dissolved Cu^{2+} ions meet SO_4^{2-} ions, they will directly reach over saturation and crystallize out $CuSO_4{\cdot}xH_2O$ (Eq. (11)). Meanwhile, due to the existence of OH^{-} from the cathode reaction, this process may be accompanied by Reaction (12), forming $Cu_4(SO_4)(OH)_6$ precipitates [1,28]. Large amounts of corrosion products accumulated at the anode plate edge, hindering the further migration process of ions. As a result, only trace

amounts of Ag^+ and Cu^{2+} can eventually migrate out and combine with OH^- from the cathode plate to form precipitates ($Cu(OH)_2$, CuO, Ag_2O, etc.), which is entirely consistent with the element distribution mapping results (Fig. 3).

$$Cu^{2+}+SO_4^{2-}+xH_2O \rightarrow CuSO_4 \cdot xH_2O \quad (11)$$

$$4Cu^{2+}+SO_4^{2-}+6OH^- \rightarrow CuSO_4 \cdot 3Cu(OH)_2 (\text{or } Cu_4(SO_4)(OH)_6) \quad (12)$$

The ECM model for PCB-HASL is shown in Fig. 13. Similar to PCB-ImAg, directional migration of specific ions occurs. The difference is that the Sn plating layer is also involved in the ECM process, in form of Sn^{4+} ions. In the initial stage of ECM process, the Sn plating layer of the anode plate dissolves first, and the main reactions are shown in Eqs. (13)−(15):

$$Sn \rightarrow Sn^{2+}+2e \quad (13)$$

$$Sn^{2+} \rightarrow Sn^{4+}+2e \quad (14)$$

$$Sn \rightarrow Sn^{4+}+4e \quad (15)$$

Under the applied electrical bias, most of Sn^{2+} will be further oxidized to Sn^{4+} [29]. Due to the large charge number carried by Sn^{4+}, it has a high migration rate and can quickly migrate to the cathode plate. As a result, a portion of Sn^{4+} ions are reduced directly to metal Sn (Eq. (16)) on the cathode plate, while the other portion is precipitated as $Sn(OH)_4$ (Eq. (17)) [30]. Under the absorbed thin liquid film, the strong oxygen reduction reaction will result in a high concentration of OH^- ions on the cathode plate surface. $Sn(OH)_4$ and even metal Sn may further dissolve through Reactions (18) and (19), along with the thinning of the Sn plating layer. This will greatly reduce the protective effect of the Sn plating layer on the substrate.

$$Sn^{4+} \rightarrow Sn-4e \quad (16)$$

$$Sn^{4+}+4OH^- \rightarrow Sn(OH)_4 \quad (17)$$

$$Sn(OH)_4+2NaOH \rightarrow Na_2Sn(OH)_6 \quad (18)$$

$$Sn+2NaOH+4H_2O \rightarrow Na_2Sn(OH)_6+2H_2 \quad (19)$$

With the dissolving of the Sn plating layer on the anode plate, the Cu substrate is gradually exposed and involved in the ECM process. As a result of plating out of Sn^{4+} on the cathode plate, the distance between two plates is dramatically shortened and the electric field intensity is enhanced accordingly. Large amounts of dissolved Cu^{2+} ions become the main part of the migration ions and reach the central position between two plates quickly, where part ions crystallize out as $CuSO_4 \cdot xH_2O$, while the other part ions are reduced directly to Cu dendrites (Fig. 4(b)), causing a short-circuit failure.

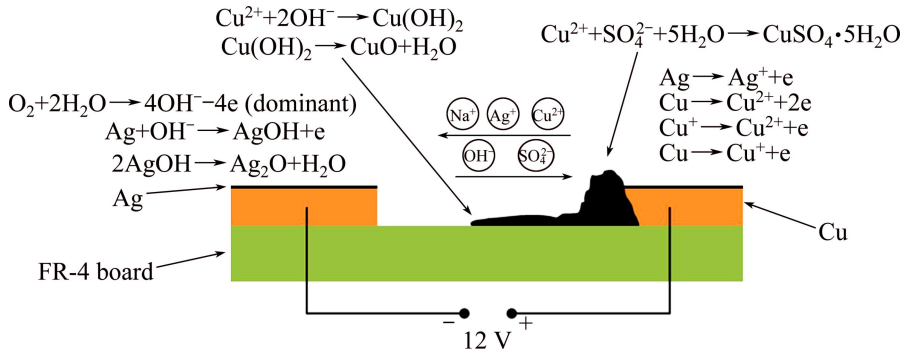

Fig. 12 ECM model for PCB-ImAg

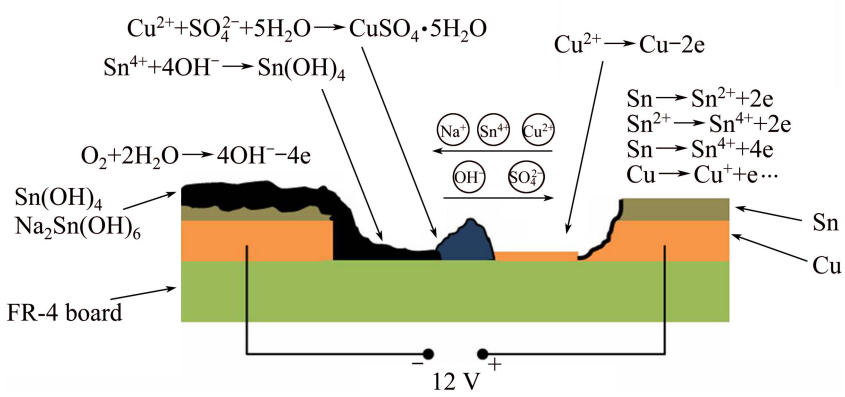

Fig. 13 ECM model for PCB-HASL

4 Conclusions

1) When applied with an electrical bias of 12 V, ECM occurred for PCB. Under different humidity conditions, the amount of migrating corrosion products of silver for PCB-ImAg was limited, while on PCB-HASL both copper dendrites and precipitates such as sulfate and metal oxides of copper/tin appeared under a high humidity condition (exceeding 85% RH).

2) For both kinds of PCB materials, the corrosion resistance of the cathode plates changed significantly after bias application, with a higher corrosion tendency.

3) Compared with PCB-ImAg, PCB-HASL had a high ECM tendency and a short-circuit failure would occur under high humidity conditions. The accumulation of corrosion products on the anode plate of PCB-ImAg hindered the further migration of Ag^+ and Cu^{2+}, limiting the migration amount of corrosion products.

References

[1] LEYGRAF C, GRAEDEL T. Atmospheric corrosion [M]. New York: John Wiley & Sons, 2000: 142−151.

[2] HUANG Hua-liang, PAN Zhi-quan, GUO Xing-peng, QIU Yu-bing. Effects of direct current electric field on corrosion behaviour of copper, Cl^- ion migration behaviour and dendrites growth under thin electrolyte layer [J]. Transactions of Nonferrous Metals Society of China, 2014, 24(1): 285−291.

[3] MEDGYES B, ILLÉS B, BERÉNYI R, HARSÁNYI G. In situ optical inspection of electrochemical migration during THB tests [J]. Journal of Materials Science: Materials in Electronics, 2011, 22(6): 694−700.

[4] RUDRA B, JENNINGS D. Failure-mechanism models for conductive-filament formation [J]. IEEE Transactions on Reliability, 1994, 43(3): 354−360.

[5] READY W J, TURBINI L J. The effect of flux chemistry, applied voltage, conductor spacing, and temperature on conductive anodic filament formation [J]. Journal of Electronic Materials, 2002, 31(11): 1208−1224.

[6] DEVOS O, GABRIELLI C, BEITONE L, MACE C, OSTERMANN E, PERROT H. Growth of electrolytic copper dendrites II: Oxalic acid medium [J]. Journal of Electroanalytical Chemistry, 2007, 606(2): 85−94.

[7] GABRIELLI C, BEITONE L, MACE C, OSTERMANN E, PERROT H. Electrochemistry on microcircuits II: Copper dendrites in oxalic acid [J]. Microelectronic Engineering, 2008, 85(8): 1686−1698.

[8] WANG Guang-jun, WANG De-zhi. Development of copper coatings on molybdenum powders by electroless plating technique [J]. Transactions of Nonferrous Metals Society of China, 2007, 17(S1): s803−s807.

[9] WU Hong-yan, ZHOU Qiong-yu, ZHONG Qing-dong, SHENG Min-qi, WANG Yi, LIN Hai. Effect of F^- on corrosion electrochemical behavior of copper in 5% Na_2SO_4 solution by using electrode array [J]. The Chinese Journal of Nonferrous Metals, 2011, 21(7): 1614−1622. (in Chinese)

[10] CUI Zhong-yu, XIAO Kui, DONG Chao-fang, DING Yuan, WANG Tao, LI Xiao-gang. Corrosion behavior of copper and brass in serious Xisha marine atmosphere [J]. The Chinese Journal of Nonferrous Metals, 2013, 23(3): 742−749. (in Chinese)

[11] WANG W, CHOUBEY A, AZARIAN M H, PECHT M. An assessment of immersion silver surface finish for lead-free electronics [J]. Journal of Electronic Materials, 2009, 38(6): 815−827.

[12] CHAIKIN S, JANNEY J, CHURCH F, MCCLELLAND C. Silver migration and printed wiring [J]. Industrial & Engineering Chemistry, 1959, 51(3): 299−304.

[13] YANG S, CHRISTOU A. Failure model for silver electrochemical migration [J]. IEEE Transactions on Device and Materials Reliability, 2007, 7(1): 188−196.

[14] LEE B Z, LEE D N. Spontaneous growth mechanism of tin whiskers [J]. Acta Materialia, 1998, 46(10): 3701−3714.

[15] ZOU S, LI X, DONG C, DING K, XIAO K. Electrochemical migration, whisker formation, and corrosion behavior of printed circuit board under wet H_2S environment [J]. Electrochimica Acta, 2013, 114: 363−371.

[16] LEE A, MAMRICK M. Fretting corrosion of tin-plated copper alloy [J]. IEEE Transactions on Components, Hybrids, and Manufacturing Technology, 1987, 10(1): 63−67.

[17] LEE S B, YOO Y R, JUNG J Y, PARK Y B, KIM Y S, JOO Y C. Electrochemical migration characteristics of eutectic SnPb solder alloy in printed circuit board [J]. Thin Solid Films, 2006, 504(1): 294−297.

[18] HARSÁNYI G. Electrochemical processes resulting in migrated short failures in microcircuits [J]. IEEE Transactions on Components, Packaging, and Manufacturing Technology: Part A, 1995, 18(3): 602−610.

[19] HARSÁNYI G, INZELT G. Comparing migratory resistive short formation abilities of conductor systems applied in advanced interconnection systems [J]. Microelectronics Reliability, 2001, 41(2): 229−237.

[20] WAN Ye, WANG Xiu-mei, ZHANG Yang, LIU Si-yu, SUN Hong. Electrochemical behavior of silver in NaOH solution [J]. The Chinese Journal of Nonferrous Metals, 2014, 24(2): 535−541. (in Chinese)

[21] FRANEY J P, KAMMLOTT G W, GRAEDEL T E. The corrosion of silver by atmospheric sulfurous gases [J]. Corrosion Science, 1985, 25(2): 133−143.

[22] STRATMANN M. The investigation of the corrosion properties of metals covered with adsorbed electrolyte layers — A new experimental technique [J]. Corrosion Science, 1987, 27(8): 869−872.

[23] STRATMANN M, STRECKEL H. On the atmospheric corrosion of metals which are covered with thin electrolyte layers—I. Verification of the experimental technique [J]. Corrosion Science, 1990, 30 (6−7): 681−696.

[24] STRATMANN M, STRECKEL H. On the atmospheric corrosion of metals which are covered with thin electrolyte layers — II. Experimental results [J]. Corrosion Science, 1990, 30(6−7): 697−714.

[25] JOUEN S, HANNOYER B, PIANA O. Non-destructive surface analysis applied to atmospheric corrosion of tin [J]. Surface and Interface Analysis, 2002, 34(1): 192−196.

[26] STRATMANN M, STRECKEL H, KIM K T, CROCKETT S. On the atmospheric corrosion of metals which are covered with thin electrolyte layers—III. The measurement of polarisation curves on metal surfaces which are covered by thin electrolyte layers [J]. Corrosion Science, 1990, 30(6−7): 715−734.

[27] ZHONG X, ZHANG G, QIU Y, CHEN Z, ZOU W, GUO X. In situ study the dependence of electrochemical migration of tin on chloride [J]. Electrochemistry Communications, 2013, 27: 63−68.

[28] FITZGERALD K P, NAIRN J, SKENNERTON G, ATRENS A. Atmospheric corrosion of copper and the colour, structure and

composition of natural patinas on copper [J]. Corrosion Science, 2006, 48(9): 2480−2509.

[29] MINZARI D, JELLESEN M S, MØLLER P, AMBAT R. On the electrochemical migration mechanism of tin in electronics [J]. Corrosion Science, 2011, 53(10): 3366−3379.

[30] YAN Zhong, XIAN Ai-ping. Initial corrosion behavior of Sn and Sn−3Ag−0.5Cu alloy exposed in atmospheric environment of Shenyang [J]. The Chinese Journal of Nonferrous Metals, 2012, 22(5): 1398−1406. (in Chinese)

吸附薄液膜下 PCB-ImAg 和 PCB-HASL 电化学迁移腐蚀行为与机理

丁康康，李晓刚，肖 葵，董超芳，张 凯，赵瑞涛

北京科技大学 腐蚀与防护中心，北京 100083

摘 要：采用体视学显微镜和扫描电镜(SEM)结合 X 射线能谱分析(EDS)研究不同厚度 0.1 mol/L Na_2SO_4 薄液膜下浸银处理电路板(PCB-ImAg)和无电镀镍金处理电路版(PCB-ENIG)的电化学迁移行为与机理，结合交流阻抗谱(EIS)和扫描 Kelvin 探针技术(SKP)对电偏压作用后 PCB 金属极板的腐蚀倾向和动力学规律进行分析。研究结果表明，经电偏压作用后，在不同湿度条件下，PCB-ImAg 板上银的迁移腐蚀产物数量极为有限，而在高湿度条件下(85%)下，PCB-HASL 两电极间同时发现了铜枝晶以及铜/锡的硫酸盐、金属氧化物等沉积物。SKP 结果表明，阴极板表面电位明显低于阳极板表面电位，具有较高的腐蚀倾向。建立电偏压作用下 PCB 电化学迁移腐蚀反应机理模型，并对两种电路板电化学迁移行为差异进行比较。

关键词：浸银电路板；无铅热风整平喷锡电路板；电化学迁移；电偏压；吸附薄液膜

(Edited by Xiang-qun LI)